



ELSEVIER

Available online at www.sciencedirect.com

SCIENCE @ DIRECT®

Journal of Sound and Vibration 285 (2005) 547–569

JOURNAL OF
SOUND AND
VIBRATION

www.elsevier.com/locate/jsvi

Three-dimensional modelling and dynamic analysis of an automatic ball balancer in an optical disk drive

Wonsuk Kim^{a,1}, Dong-Jin Lee^{b,2}, Jintai Chung^{b,*}

^a*BK 21 Division for Research and Education in Mechanical Engineering, Hanyang University,
17 Haengdang-dong, Seongdong-gu, Seoul 133-791, South Korea*

^b*Department of Mechanical Engineering, Hanyang University, 1271 Sa-1-dong, Ansan, Kyunggi-do 425-791, South Korea*

Received 5 December 2002; received in revised form 18 February 2004; accepted 26 August 2004

Available online 23 November 2004

Abstract

Dynamic behaviours and stability of an automatic ball balancer (ABB) in an optical disk drive are analyzed based on the proposed three-dimensional dynamic model. For dynamic analysis, the feeding deck with the ball balancer and a spindle motor is modelled as a rigid body with six degrees of freedom. The nonlinear equations of motion are derived using Lagrange's equation in order to describe the translational and rotational motions of the system. From the derived nonlinear equations, the linearized equations of motion in the neighbourhood of a balanced equilibrium position are obtained by the perturbation method. These equations are coupled, linear, differential equations with time-dependent periodic coefficients, from which the stability of the system is analyzed by using the Floquet theory. Finally, the time responses are computed to verify the results of the stability analysis, and to investigate the balancing performance of the ABB.

© 2004 Elsevier Ltd. All rights reserved.

*Corresponding author. Tel.: +82 31 400 5287; fax: +82 31 406 5550.
E-mail address: jchung@hanyang.ac.kr (J. Chung).

¹Currently with the University of Michigan-Dearborn, USA.

²Currently with Samsung Electronics Co., South Korea.

1. Introduction

Most manufacturers of high-speed optical disk drives, such as CD-ROM or DVD drives, nowadays adopt an automatic ball balancer (ABB) to automatically reduce the variable imbalance of rotating mechanisms. This imbalance is usually a result of unavoidable imperfection in the manufacturing and assembling processes of an optical disk and a spindle motor. Once in a while, mistakes during data recording and labelling on a disk can also be a source of imperfection. Under these circumstances, it is impossible to make rotating systems balanced by only one time of balancing at an initial stage because the amount of imbalance varies depending on operating conditions. The ABB are thus widely used for the purpose of resolving the difficulty.

Although various types of automatic balancers are used in not only optical disk drives but also many other application areas, e.g., washing machines [1] and machining tools [2], not many studies have been reported. The basic research was initiated by Alexander [3] and Cade [4] in the 1960s. In the 1990s, while Lee and Van Moorhem [5] analyzed the dynamic behaviour of automatic balancers for a non-autonomous system, Chung and Ro [6] and Hwang and Chung [7] studied the Jeffcott rotor from the standpoint of an autonomous system by using polar coordinates instead of rectangular coordinates. However, since most of the previous studies focused on an automatic balancer itself, there are very few studies for an optical disk drive with the ABB.

The performance of the ABB installed in an optical disk drive was recently evaluated by Kang et al. [8], Huang et al. [9] and Kim and Chung [10]. In these studies, after the equations of motion were derived from the two-dimensional mathematical models of the ABB and feeding deck, the stability and parametric analyses were performed using various methods to obtain the design guidelines of ABBs. However, the influence of the out-of-plane tilting motions of a feeding deck on the balancing performance of the ABB could not be evaluated because the analyses were based on the two-dimensional, in-plane models. Regarding non-planar dynamic modelling and analysis, one available work is that of Chao et al. [11]. In their study, the radial vibration and the tilting motion of the rotor-disk assembly were calculated by numerical integrations.

In this paper, a three-dimensional, mathematical model of an ABB in a commercial optical disk drive is developed considering not only the in-plane but also the out-of-plane translational and rotational motions of the feeding deck. Based on the model, the nonlinear equations of motion for a non-autonomous system are derived using Lagrange's equation. Applying the perturbation method to the nonlinear equations, the linearized equations of motion in the neighbourhood of a balanced equilibrium position are obtained. Next, for various design parameters, the stability analyses are performed by using the Floquet theory. Finally, time responses are calculated to verify the stability plots and to show the effectiveness of the ABB. Some issues regarding the out-of-plane and the in-plane motions are also discussed.

2. Modelling and nonlinear equations of motion

The ABB is comprised of an annular structure with a race containing a viscous damping fluid and a plurality of spherical balls as shown in Fig. 1. The balancing balls are freely movable in the race. The ABB and the rotor of a spindle motor are assembled into a single body, so that they are

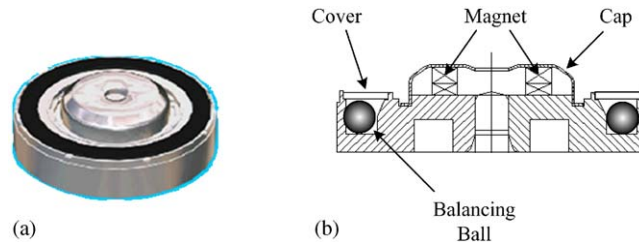


Fig. 1. ABB for an optical disk drive: (a) the three-dimensional view, (b) the cross-sectional view.

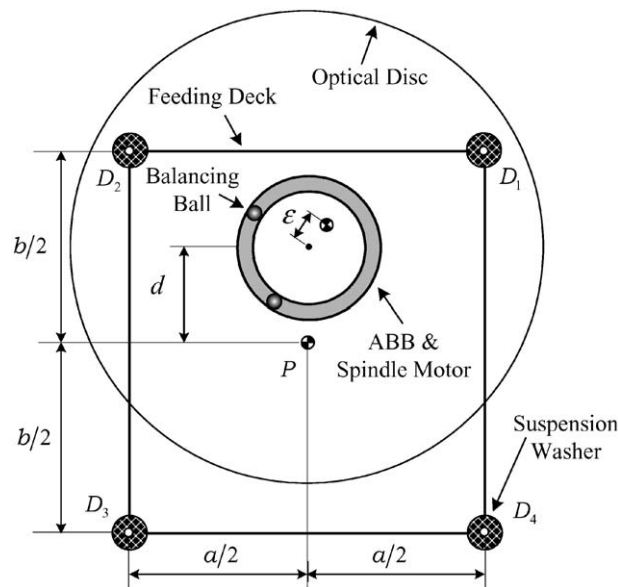


Fig. 2. Schematic of the ABB installed in an optical disk drive (not drawn to scale).

rotating at a constant angular speed ω . Since the ABB plays an additional role of the conventional turntable, an optical disk is put on the ABB and it is fixed between the ABB and the magnetic clamber.

Shown in Fig. 2 is a schematic of the ABB installed in an optical disk drive. The stationary part of the spindle motor is rigidly fixed on the feeding deck which is mounted on the base of the optical disk drive by four suspension washers. Each suspension washer is modelled as an equivalent linear spring and damper. Points C and G denote the rotation centre and the mass centre, respectively, of the rotor system including the ABB, the spindle motor and the optical disk. In general, points C and G do not coincide with each other because the rotor system may have mass unbalancing. The distance ϵ between C and G is known as the mass eccentricity. For the simplicity of analysis the feeding deck is assumed as a uniform thin rectangular plate, where width and length are a and b , respectively; hence, the mass centre P of the feeding deck coincides with the geometric centre of the plate. The distance between points P and C is given by d .

It is also assumed in this article that the mass centre of the feeding deck P and the mass centre of the rotor system G are located on the same plane, because the latest commercial optical disk drives are very slim. If the locations of the mass centres of the feeding deck, the balancing balls, the spindle motor and the optical disk cannot be assumed to be on the same plane, a slightly different model needs to be developed. To researchers who want to pursue this direction the authors recommend the recent work by Chao et al. [11], in which one can find how to efficiently model that case, and one can also evaluate the influence of the mass-centre offsets on the tilting motion of the rotor-disk assembly.

In this study, to consider both the in-plane and the out-of-plane motions, the feeding deck is modelled as a rigid body with six degrees of freedom: three translational and three rotational ones. As shown in Fig. 3, the Euler angles γ , α and β are used to describe the rotational motion of the system in the three-dimensional space. The XYZ coordinate system is a space-fixed inertial reference frame. A rotation γ about the Z -axis puts the system into an orientation coincident with the primed $x'y'z'$ coordinate system, and a further rotation α about the x' -axis results in the double-primed $x''y''z''$ coordinate system. Finally, the third rotation β about the y'' -axis yields the xyz coordinate system that is fixed on the feeding deck. These coordinate transformations can be arranged in matrix form as follows:

$$\mathbf{x}' = \mathbf{T}_\gamma \mathbf{X}, \quad \mathbf{x}'' = \mathbf{T}_\alpha \mathbf{x}', \quad \mathbf{x} = \mathbf{T}_\beta \mathbf{x}'', \quad (1)$$

where

$$\mathbf{T}_\gamma = \begin{bmatrix} \cos \gamma & \sin \gamma & 0 \\ -\sin \gamma & \cos \gamma & 0 \\ 0 & 0 & 1 \end{bmatrix}, \quad \mathbf{T}_\alpha = \begin{bmatrix} 1 & 0 & 0 \\ 0 & \cos \alpha & \sin \alpha \\ 0 & -\sin \alpha & \cos \alpha \end{bmatrix}, \quad \mathbf{T}_\beta = \begin{bmatrix} \cos \beta & 0 & -\sin \beta \\ 0 & 1 & 0 \\ \sin \beta & 0 & \cos \beta \end{bmatrix}, \quad (2)$$

$$\mathbf{X} = X\mathbf{I} + Y\mathbf{J} + Z\mathbf{K}, \quad \mathbf{x}' = x'\mathbf{i}' + y'\mathbf{j}' + z'\mathbf{k}', \quad \mathbf{x}'' = x''\mathbf{i}'' + y''\mathbf{j}'' + z''\mathbf{k}'', \quad \mathbf{x} = x\mathbf{i} + y\mathbf{j} + z\mathbf{k}, \quad (3)$$

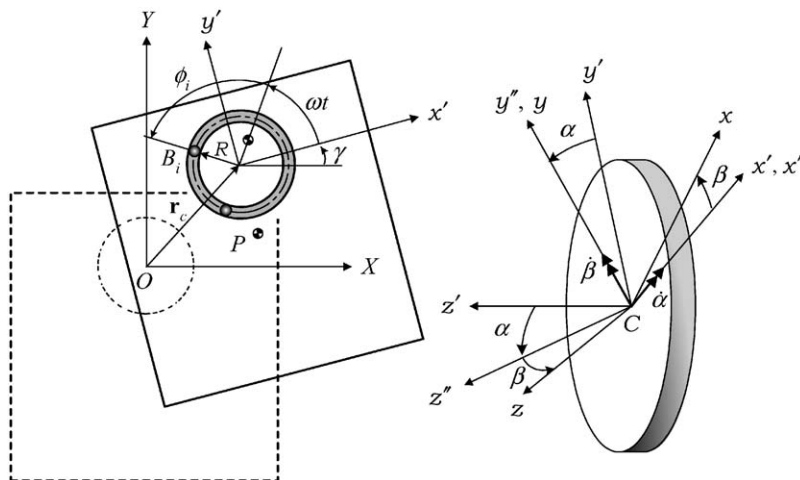


Fig. 3. Configuration of the ABB and the Euler angles to describe the rotational motions.

in which \mathbf{I} , \mathbf{J} and \mathbf{K} are the unit vectors along the X -, Y - and Z -axis; \mathbf{i}' , \mathbf{j}' and \mathbf{k}' are the unit vectors along the x' -, y' - and z' -axis; \mathbf{i}'' , \mathbf{j}'' and \mathbf{k}'' are the unit vectors along the x'' -, y'' - and z'' -axis; and \mathbf{i} , \mathbf{j} and \mathbf{k} are the unit vectors along the x -, y - and z -axis, respectively. As a result, the orientation of the feeding deck with respect to the inertial reference frame can be expressed by the angles α , β and γ . On the other hand, the translational motion of the feeding deck is represented by the displacement vector \mathbf{r}_c in Fig. 3. Also, the angular position of the i th balancing ball B_i can be described by the pitch radius R of the race and the angle ϕ_i with respect to the angular position of G .

First, the kinetic energy of the system is considered. The position vector of the mass centre G can be expressed in the xyz coordinate system by using the rotation matrices \mathbf{T}_γ , \mathbf{T}_α and \mathbf{T}_β :

$$\mathbf{r}_G = \mathbf{T}_\beta \mathbf{T}_\alpha \mathbf{T}_\gamma \mathbf{r}_{C/XYZ} + \mathbf{r}_{CG/xyz}, \tag{4}$$

where

$$\mathbf{r}_{C/XYZ} = X\mathbf{I} + Y\mathbf{J} + Z\mathbf{K}, \quad \mathbf{r}_{CG/xyz} = \varepsilon(\cos \omega t \mathbf{i} + \sin \omega t \mathbf{j}), \tag{5}$$

in which t is time. By substituting Eqs. (2) and (5) into Eq. (4), \mathbf{r}_G can be expressed as

$$\begin{aligned} \mathbf{r}_G = & [X(\cos \beta \cos \gamma - \sin \alpha \sin \beta \sin \gamma) + Y(\sin \alpha \sin \beta \cos \gamma + \cos \beta \sin \gamma) \\ & + Z \cos \alpha \sin \beta + \varepsilon \cos \omega t] \mathbf{i} + [-X \cos \alpha \sin \gamma + Y \cos \alpha \cos \gamma + Z \sin \alpha + \varepsilon \sin \omega t] \mathbf{j} \\ & + [X(\sin \beta \cos \psi + \sin \alpha \cos \beta \sin \gamma) + Y(-\sin \alpha \cos \beta \cos \gamma + \sin \beta \sin \gamma) \\ & + Z \cos \alpha \cos \beta] \mathbf{k}. \end{aligned} \tag{6}$$

Similarly, the position vector of the i th ball, \mathbf{r}_{B_i} , and the position vector of point P , \mathbf{r}_P , may be written as

$$\begin{aligned} \mathbf{r}_{B_i} = & [X(\cos \beta \cos \gamma - \sin \alpha \sin \beta \sin \gamma) + Y(\sin \alpha \sin \beta \cos \gamma + \cos \beta \sin \gamma) \\ & + Z \cos \alpha \sin \beta + R \cos(\phi_i + \omega t)] \mathbf{i} + [-X \cos \alpha \sin \gamma + Y \cos \alpha \cos \gamma \\ & + Z \sin \alpha + R \sin(\phi_i + \omega t)] \mathbf{j} + [X(\sin \beta \cos \psi + \sin \alpha \cos \beta \sin \gamma) \\ & + Y(-\sin \alpha \cos \beta \cos \gamma + \sin \beta \sin \gamma) + Z \cos \alpha \cos \beta] \mathbf{k}, \end{aligned} \tag{7}$$

$$\begin{aligned} \mathbf{r}_P = & [X(\cos \beta \cos \gamma - \sin \alpha \sin \beta \sin \gamma) + Y(\sin \alpha \sin \beta \cos \gamma + \cos \beta \sin \gamma) \\ & + Z \cos \alpha \sin \beta] \mathbf{i} + [-X \cos \alpha \sin \gamma + Y \cos \alpha \cos \gamma + Z \sin \alpha - d] \mathbf{j} \\ & + [X(\sin \beta \cos \psi + \sin \alpha \cos \beta \sin \gamma) + Y(-\sin \alpha \cos \beta \cos \gamma + \sin \beta \sin \gamma) \\ & + Z \cos \alpha \cos \beta] \mathbf{k}. \end{aligned} \tag{8}$$

On the other hand, the angular velocity vectors of the rotor and feeding deck, $\boldsymbol{\omega}_G$ and $\boldsymbol{\omega}_P$, respectively, are given by

$$\boldsymbol{\omega}_G = (\dot{\alpha} \cos \beta - \dot{\gamma} \cos \alpha \sin \beta) \mathbf{i} + (\dot{\beta} + \dot{\gamma} \sin \alpha) \mathbf{j} + (\dot{\alpha} \sin \beta + \dot{\gamma} \cos \alpha \cos \beta + \omega) \mathbf{k}, \tag{9}$$

$$\boldsymbol{\omega}_P = (\dot{\alpha} \cos \beta - \dot{\gamma} \cos \alpha \sin \beta) \mathbf{i} + (\dot{\beta} + \dot{\gamma} \sin \alpha) \mathbf{j} + (\dot{\alpha} \sin \beta + \dot{\gamma} \cos \alpha \cos \beta) \mathbf{k}. \tag{10}$$

When the ABB has n balls, whose masses and sizes are all the same, the kinetic energy T is then given by

$$T = \frac{1}{2} M \frac{d\mathbf{r}_G}{dt} \cdot \frac{d\mathbf{r}_G}{dt} + \frac{1}{2} M_P \frac{d\mathbf{r}_P}{dt} \cdot \frac{d\mathbf{r}_P}{dt} + \frac{1}{2} \boldsymbol{\omega}_G^T \mathbf{J}_G \boldsymbol{\omega}_G + \frac{1}{2} \boldsymbol{\omega}_P^T \mathbf{J}_P \boldsymbol{\omega}_P + \frac{1}{2} m \sum_{i=1}^n \frac{d\mathbf{r}_{B_i}}{dt} \cdot \frac{d\mathbf{r}_{B_i}}{dt}, \quad (11)$$

where M , M_P and m are masses of the rotor system, the feeding deck and each balancing ball; and \mathbf{J}_G and \mathbf{J}_P are the inertia matrices of the rotor system and the feeding deck. Note that the mass moment of inertia of the balancing ball is neglected because the ball is very small. The inertia matrices \mathbf{J}_G and \mathbf{J}_P can be written in matrix form

$$\mathbf{J}_G = \begin{bmatrix} J_x & 0 & 0 \\ 0 & J_y & 0 \\ 0 & 0 & J_z \end{bmatrix}, \quad \mathbf{J}_P = \begin{bmatrix} J_{Px} & 0 & 0 \\ 0 & J_{Py} & 0 \\ 0 & 0 & J_{Pz} \end{bmatrix}, \quad (12)$$

in which J_x, J_y or J_z is the mass moment of inertia of the rotor system about the x -, y - or z -axis; J_{Px}, J_{Py} or J_{Pz} is the mass moment of inertia of the feeding deck about an axis which is passing through point P and parallel to the x -, y - or z -axis, respectively.

Now, let us consider the potential energy of the system. Neglecting gravity, the potential energy can be computed from

$$V = \frac{1}{2} k \sum_{i=1}^4 \mathbf{r}_{D_i} \cdot \mathbf{r}_{D_i}. \quad (13)$$

In the above, \mathbf{r}_{D_i} is the displacement vector of the each corner of the feeding deck where the suspension washer is attached, and k is the equivalent stiffness of the suspension washer. It is assumed that the stiffness is the same regardless of orientation. The deformation of four washers can be expressed as

$$\mathbf{r}_{D_i} = \mathbf{T}_\beta \mathbf{T}_\alpha \mathbf{T}_\gamma \mathbf{r}_{C/XYZ} + \mathbf{r}_{CD_i/xyz} - \mathbf{T}_\beta \mathbf{T}_\alpha \mathbf{T}_\gamma \mathbf{r}_{OD_i/XYZ}, \quad i = 1, 2, 3, 4, \quad (14)$$

where

$$\begin{aligned} \mathbf{r}_{CD_1/xyz} &= \frac{a}{2} \mathbf{i} + \left(\frac{b}{2} - d\right) \mathbf{j}, & \mathbf{r}_{CD_2/xyz} &= -\frac{a}{2} \mathbf{i} + \left(\frac{b}{2} - d\right) \mathbf{j}, & \mathbf{r}_{CD_3/xyz} &= -\frac{a}{2} \mathbf{i} - \left(\frac{b}{2} + d\right) \mathbf{j}, \\ \mathbf{r}_{CD_4/xyz} &= \frac{a}{2} \mathbf{i} - \left(\frac{b}{2} + d\right) \mathbf{j}, & \mathbf{r}_{OD_1/XYZ} &= \frac{a}{2} \mathbf{I} + \left(\frac{b}{2} - d\right) \mathbf{J}, & \mathbf{r}_{OD_2/XYZ} &= -\frac{a}{2} \mathbf{I} + \left(\frac{b}{2} - d\right) \mathbf{J}, \\ \mathbf{r}_{OD_3/XYZ} &= -\frac{a}{2} \mathbf{I} - \left(\frac{b}{2} + d\right) \mathbf{J}, & \mathbf{r}_{OD_4/XYZ} &= \frac{a}{2} \mathbf{I} - \left(\frac{b}{2} + d\right) \mathbf{J}. \end{aligned} \quad (15)$$

On the other hand, Rayleigh's dissipation function F is given by

$$F = \frac{1}{2} c \sum_{i=1}^4 \frac{d\mathbf{r}_{D_i}}{dt} \cdot \frac{d\mathbf{r}_{D_i}}{dt} + \frac{1}{2} D \sum_{i=1}^n \dot{\phi}_i^2, \quad (16)$$

where D is the viscous drag coefficient of the balancing ball in the damping fluid, and c is the equivalent damping coefficient of the suspension washer. Rubber, plastic, or metal is typically used as a damping material of the suspension washer in optical disk drives [8,9].

The equations of motion for the system are now derived using Lagrange’s equation given by

$$\frac{d}{dt} \left(\frac{\partial T}{\partial \dot{q}_k} \right) - \frac{\partial T}{\partial q_k} + \frac{\partial V}{\partial q_k} + \frac{\partial F}{\partial \dot{q}_k} = 0, \tag{17}$$

where q_k are the generalized coordinates. Choose as generalized coordinates $X, Y, Z, \alpha, \beta, \gamma$ and ϕ_i ($i = 1, 2, \dots, n$); therefore, the dynamic behaviour of the system is governed by $n + 6$ independent equations of motion. Substitution of Eqs. (11), (13) and (16) into Eq. (17) yields the equations of motion. Assuming that $X, Y, Z, \alpha, \beta,$ and γ are small, the simplified governing equations are obtained as follows:

$$\begin{aligned} (M + M_P + nm)\ddot{X} + 4c\dot{X} + 4kX + (M_P d - M\varepsilon \sin \omega t)\ddot{\gamma} + (4dc - 2M\varepsilon\omega \cos \omega t)\dot{\gamma} \\ + (4dk + M\varepsilon\omega^2 \sin \omega t)\gamma - mR \sum_{i=1}^n \{[\ddot{\gamma} + \ddot{\phi}_i - (\dot{\phi}_i + \omega)^2\gamma] \sin(\phi_i + \omega t) \\ + [\gamma\ddot{\phi}_i + (\dot{\phi}_i + \omega)(2\dot{\gamma} + \dot{\phi}_i + \omega)] \cos(\phi_i + \omega t)\} = M\varepsilon\omega^2 \cos \omega t, \end{aligned} \tag{18}$$

$$\begin{aligned} (M + M_P + nm)\ddot{Y} + 4c\dot{Y} + 4kY + M\varepsilon \cos \omega t\ddot{\gamma} - 2M\varepsilon\omega \sin \omega t\dot{\gamma} - M\varepsilon\omega^2 \cos \omega t\gamma \\ + mR \sum_{i=1}^n \{[\ddot{\gamma} + \ddot{\phi}_i - (\dot{\phi}_i + \omega)^2\gamma] \cos(\phi_i + \omega t) \\ - [\gamma\ddot{\phi}_i + (\dot{\phi}_i + \omega)(2\dot{\gamma} + \dot{\phi}_i + \omega)] \sin(\phi_i + \omega t)\} = M\varepsilon\omega^2 \sin \omega t, \end{aligned} \tag{19}$$

$$\begin{aligned} (M + M_P + nm)\ddot{Z} + 4c\dot{Z} + 4kZ - (M_P d - M\varepsilon \sin \omega t)\ddot{\alpha} - (4dc - 2M\varepsilon\omega \cos \omega t)\dot{\alpha} - 4dk\alpha \\ - M\varepsilon\ddot{\beta} \cos \omega t + 2M\varepsilon\omega\dot{\beta} \sin \omega t + mR \sum_{i=1}^n \{[-\ddot{\beta} + \alpha\ddot{\phi}_i + 2(\dot{\phi}_i + \omega)\dot{\alpha} + (\dot{\phi}_i + \omega)^2\beta] \cos(\phi_i + \omega t) \\ + [\ddot{\alpha} + \beta\ddot{\phi}_i + 2(\dot{\phi}_i + \omega)\dot{\beta} - (\dot{\phi}_i + \omega)^2\alpha] \sin(\phi_i + \omega t)\} = M\varepsilon\omega^2(\alpha \sin \omega t - \beta \cos \omega t), \end{aligned} \tag{20}$$

$$\begin{aligned} \left[J_x + J_{P_x} + M_P d^2 + M\varepsilon^2 \sin^2 \omega t + mR^2 \sum_{i=1}^n \sin^2(\phi_i + \omega t) \right] \ddot{\alpha} \\ + \left[(b^2 + 4d^2)c + 2M\varepsilon^2\omega \sin \omega t \cos \omega t + 2mR^2 \sum_{i=1}^n (\dot{\phi}_i + \omega) \sin(\phi_i + \omega t) \cos(\phi_i + \omega t) \right] \dot{\alpha} \\ + (b^2 + 4d^2)k\alpha - \left[M\varepsilon^2 \sin \omega t \cos \omega t + mR^2 \sum_{i=1}^n \sin(\phi_i + \omega t) \cos(\phi_i + \omega t) \right] \ddot{\beta} \end{aligned}$$

$$\begin{aligned}
& + \left[J_z \omega + 2M\varepsilon^2 \omega \sin^2 \omega t + 2mR^2 \sum_{i=1}^n (\dot{\phi}_i + \omega) \sin^2(\phi_i + \omega t) \right] \dot{\beta} + mR^2 \beta \sum_{i=1}^n \ddot{\phi}_i \\
& + \left[-Mpd + M\varepsilon \sin \omega t + mR \sum_{i=1}^n \sin(\phi_i + \omega t) \right] \ddot{Z} - 4dc\dot{Z} - 4dkZ = 0, \tag{21}
\end{aligned}$$

$$\begin{aligned}
& \left[J_y + J_{P_y} + M\varepsilon^2 \cos^2 \omega t + mR^2 \sum_{i=1}^n \cos^2(\phi_i + \omega t) \right] \ddot{\beta} \\
& + \left[a^2 c - 2M\varepsilon^2 \omega \sin \omega t \cos \omega t - 2mR^2 \sum_{i=1}^n (\dot{\phi}_i + \omega) \sin(\phi_i + \omega t) \cos(\phi_i + \omega t) \right] \dot{\beta} + a^2 k \beta \\
& - \left[M\varepsilon^2 \sin \omega t \cos \omega t + mR^2 \sum_{i=1}^n \sin(\phi_i + \omega t) \cos(\phi_i + \omega t) \right] \ddot{\alpha} \\
& - \left[J_z \omega + 2M\varepsilon^2 \omega \cos^2 \omega t + 2mR^2 \sum_{i=1}^n (\dot{\phi}_i + \omega) \cos^2(\phi_i + \omega t) \right] \dot{\alpha} \\
& - \left[M\varepsilon \cos \omega t + mR \sum_{i=1}^n \cos(\phi_i + \omega t) \right] \ddot{Z} = 0, \tag{22}
\end{aligned}$$

$$\begin{aligned}
& [J_z + J_{P_z} + Mpd^2 + M\varepsilon^2 + nmR^2] \ddot{\gamma} + (a^2 + b^2 + 4d^2)c\dot{\gamma} + (a^2 + b^2 + 4d^2)k\gamma \\
& + \left[Mpd - M\varepsilon \sin \omega t - mR \sum_{i=1}^n \sin(\phi_i + \omega t) \right] \ddot{X} + 4dc\dot{X} + 4dkX \\
& + \left[M\varepsilon \cos \omega t + mR \sum_{i=1}^n \cos(\phi_i + \omega t) \right] \ddot{Y} + mR^2 \sum_{i=1}^n \ddot{\phi}_i = 0, \tag{23}
\end{aligned}$$

$$mR^2(\ddot{\gamma} + \ddot{\phi}_i) + D\dot{\phi}_i - mR\{\ddot{X} \sin(\phi_i + \omega t) - \ddot{Y} \cos(\phi_i + \omega t)\} = 0, \quad i = 1, 2, \dots, n. \tag{24}$$

What has to be noticed here is that the equations of motion given by Eqs. (18)–(24) are coupled nonlinear differential equations with time-dependent periodic coefficients.

3. Linearized equations

The perturbation method is used to obtain equilibrium positions and linearized equations of motion in the neighbourhood of the equilibrium positions in order to compute natural frequencies and to investigate the stability of the system. The generalized coordinates X , Y , Z , α , β , γ and ϕ_i may be replaced by

$$\begin{aligned}
X &= X^* + \Delta X, & Y &= Y^* + \Delta Y, & Z &= Z^* + \Delta Z, \\
\alpha &= \alpha^* + \Delta\alpha, & \beta &= \beta^* + \Delta\beta, & \gamma &= \gamma^* + \Delta\gamma, & \phi_i &= \phi_i^* + \Delta\phi_i, \tag{25}
\end{aligned}$$

where $X^*, Y^*, Z^*, \alpha^*, \beta^*, \gamma^*$ and ϕ_i^* are parameters to represent the equilibrium positions and $\Delta X, \Delta Y, \Delta Z, \Delta\alpha, \Delta\beta, \Delta\gamma$ and $\Delta\phi_i$ are the small perturbations of the generalized coordinates in the vicinity of the equilibrium positions. Substitution of Eq. (25) into Eqs. (18)–(24) results in the equilibrium positions and the linearized equations around the equilibrium positions.

As discussed in Refs. [6,7], the equilibrium positions of an optical disk drive with the ABB may be classified into two cases: the balanced ($X^* = Y^* = Z^* = \alpha^* = \beta^* = \gamma^* = 0$) or the unbalanced equilibrium positions. Since the balanced equilibrium position is practically more important than the unbalanced equilibrium positions in the design of the ABB, this article focuses on only the balanced equilibrium position and linearized equations about the corresponding position for the stability analysis. On the other hand, the dynamics of the ABB system for the various unbalanced ball positions is well illustrated and analyzed in Ref. [8].

When the system is balanced, the positions of the balancing balls may be calculated from

$$\frac{M\varepsilon}{mR} + \sum_{i=1}^n \cos \phi_i^* = 0, \quad \sum_{i=1}^n \sin \phi_i^* = 0. \tag{26}$$

The linearized equations of motion in the neighbourhood of the balanced equilibrium position can then be expressed in terms of $\Delta X, \Delta Y, \Delta Z, \Delta\alpha, \Delta\beta, \Delta\gamma$ and $\Delta\phi_i$. For notational simplicity, deleting Δ from $\Delta X, \Delta Y, \Delta Z, \Delta\alpha, \Delta\beta, \Delta\gamma$ and $\Delta\phi_i$, the final linearized equations can be written as

$$(M + M_P + nm)\ddot{X} + 4c\dot{X} + 4kX + d(M_P\ddot{\gamma} + 4c\dot{\gamma} + 4k\gamma) - mR \sum_{i=1}^n [(\ddot{\phi}_i - \omega^2\phi_i)\sin(\phi_i^* + \omega t) + 2\omega\dot{\phi}_i\cos(\phi_i^* + \omega t)] = 0, \tag{27}$$

$$(M + M_P + nm)\ddot{Y} + 4c\dot{Y} + 4kY + mR \sum_{i=1}^n [(\ddot{\phi}_i - \omega^2\phi_i)\cos(\phi_i^* + \omega t) - 2\omega\dot{\phi}_i\sin(\phi_i^* + \omega t)] = 0, \tag{28}$$

$$(M + M_P + nm)\ddot{Z} + 4c\dot{Z} + 4kZ - d(M_P\ddot{\alpha} + 4c\dot{\alpha} + 4k\alpha) = 0, \tag{29}$$

$$\begin{aligned} & \left[J_x + J_{P_x} + M_P d^2 + M\varepsilon^2 \sin^2 \omega t + mR^2 \sum_{i=1}^n \sin^2(\phi_i^* + \omega t) \right] \ddot{\alpha} \\ & + \left[(b^2 + 4d^2)c + 2M\varepsilon^2 \omega \sin \omega t \cos \omega t + 2mR^2 \omega \sum_{i=1}^n \sin(\phi_i^* + \omega t) \cos(\phi_i^* + \omega t) \right] \dot{\alpha} \\ & + (b^2 + 4d^2)k\alpha - \left[M\varepsilon^2 \sin \omega t \cos \omega t + mR^2 \sum_{i=1}^n \sin(\phi_i^* + \omega t) \cos(\phi_i^* + \omega t) \right] \ddot{\beta} \\ & + \left[J_z \omega + 2M\varepsilon^2 \omega \sin^2 \omega t + 2mR^2 \omega \sum_{i=1}^n \sin^2(\phi_i^* + \omega t) \right] \dot{\beta} - d(M_P\ddot{Z} + 4c\dot{Z} + 4kZ) = 0, \end{aligned} \tag{30}$$

$$\begin{aligned}
& \left[J_y + J_{P_y} + M\varepsilon^2 \cos^2 \omega t + mR^2 \sum_{i=1}^n \cos^2(\phi_i^* + \omega t) \right] \ddot{\beta} \\
& + \left[a^2 c - 2M\varepsilon^2 \omega \sin \omega t \cos \omega t - 2mR^2 \omega \sum_{i=1}^n \sin(\phi_i^* + \omega t) \cos(\phi_i^* + \omega t) \right] \dot{\beta} + a^2 k \beta \\
& - \left[M\varepsilon^2 \sin \omega t \cos \omega t + mR^2 \sum_{i=1}^n \sin(\phi_i^* + \omega t) \cos(\phi_i^* + \omega t) \right] \ddot{\alpha} \\
& - \left[J_z \omega + 2M\varepsilon^2 \omega \cos^2 \omega t + 2mR^2 \omega \sum_{i=1}^n \cos^2(\phi_i^* + \omega t) \right] \dot{\alpha} = 0, \tag{31}
\end{aligned}$$

$$\begin{aligned}
& [J_z + J_{P_z} + M_P d^2 + M\varepsilon^2 + nmR^2] \ddot{y} + (a^2 + b^2 + 4d^2) c \dot{y} + (a^2 + b^2 + 4d^2) k y \\
& + d(M_P \ddot{X} + 4c \dot{X} + 4kX) + mR^2 \sum_{i=1}^n \ddot{\phi}_i = 0, \tag{32}
\end{aligned}$$

$$mR^2(\ddot{y} + \ddot{\phi}_i) + D\dot{\phi}_i - mR\{\dot{X} \sin(\phi_i^* + \omega t) - \dot{Y} \cos(\phi_i^* + \omega t)\} = 0, \quad i = 1, 2, \dots, n. \tag{33}$$

Note that Eqs. (27)–(29) predominantly govern the translational motions of the feeding deck while Eqs. (30)–(32) govern the rotational motions. Eq. (33) is mainly related to the motions of the balancing balls.

4. Stability analysis

In order to find the parameter ranges in which the ABB is working, and to evaluate the balancing performance of the ABB, the dynamic stability of a commercial optical disk drive with an ABB is analyzed in the neighbourhood of the balanced equilibrium position. In the ABB for an optical disk drive, about ten balls are usually used. However, the stability analysis of the ten-ball case is very numerically complex because of the large degrees of freedom and various equilibrium positions. Therefore, in numerical simulations, the case of $n = 2$, i.e., the case in which the ABB has only two balancing balls, is mainly considered for simplicity of the analysis (the time responses for the case of $n = 10$ will be presented in the next section for verification). When $n = 2$, the equilibrium positions of the balancing balls calculated by Eq. (26) are

$$\phi_1^* = -\phi_2^* = -\tan^{-1} \sqrt{(2mR/M\varepsilon)^2 - 1}. \tag{34}$$

A commercial CD-ROM drive is considered as an example. Shown in Table 1 are parameter values used in numerical simulations unless other values are specified. In Table 1, the dimensions and masses for the parts of the optical disk drive are measured; the stiffness value is obtained from modal testing, and the damping values are adopted from Ref. [8]. A point to be mentioned here is that the mass m in Table 1 is not the same as the mass of an actual balancing ball. Since the number of balls in this study is assumed as two instead of ten, m is taken to be five times heavier

Table 1
Parameter values of a commercial CD-ROM drive

Parameters	Values
Width of the feeding deck, a	70 mm
Length of the feeding deck, b	110 mm
Distance between points C and P , d	30 mm
Mean radius of the automatic ball balancer, R	15 mm
Mass of the feeding-deck assembly, M_P	150 g
Mass of the equivalent rotor, M	26 g
Mass of the balancing ball, m	0.43 g
Mass moments of inertia of the feeding-deck assembly, J_{Px}	$1.43 \times 10^{-4} \text{ kg m}^2$
	J_{Py} $0.31 \times 10^{-4} \text{ kg m}^2$
	J_{Pz} $1.74 \times 10^{-4} \text{ kg m}^2$
Mass moments of inertia of the equivalent rotor, J_x	$1.46 \times 10^{-6} \text{ kg m}^2$
	J_y $1.46 \times 10^{-6} \text{ kg m}^2$
	J_z $2.93 \times 10^{-6} \text{ kg m}^2$
Stiffness of the suspension washer, k	3972 N/m
Damping coefficients of the suspension washer, c (rubber)	2.53 kg/s
	c (metal) 0.66 kg/s
Drag coefficient of the balancing ball in the fluid, D	$5 \times 10^{-6} \text{ kg m}^2/\text{s}$

than the mass of an actual ball for reality. Also, the value of the eccentricity is assumed to be $\varepsilon = 0.25$ mm unless an other value is specified.

First of all, the natural frequencies of the system when $m = \omega = 0$ are calculated from the linearized equations (27)–(32). Note that the presence of the balancing balls has effects on the natural frequencies [12]. The natural frequency related to the translational motions in the X , Y and Z directions is obtained as $\omega_0 \approx 298$ rad/s. Note that the values of the translational natural frequencies in the X , Y and Z directions are found to be almost the same because the stiffness of the suspension washer is assumed to be identical regardless of the directions. On the other hand, the natural frequencies of the rotational motions about the X -, Y - and Z -axis are calculated as $\omega_\alpha = 535$ rad/s, $\omega_\beta = 750$ rad/s and $\omega_\gamma = 577$ rad/s, respectively. It is seen that the rotational natural frequencies of the system are higher than the translational natural frequencies.

At this stage, it is valuable to note that Eqs. (27)–(33) can be divided into two independent groups. The first group consists of the coupled equations of the translational (X , Y) and rotational (γ , ϕ_i) coordinates, used to describe the in-plane motions, as shown in Eqs. (27), (28), (32) and (33). The other group is the coupled equations of the translational (Z) and rotational (α , β) coordinates, used to describe the out-of-plane motions, as shown in Eqs. (29)–(31). Since the in-plane (first group) and out-of-plane (second group) motions are decoupled with each other in the neighbourhood of the balanced equilibrium position, the stability analysis can be performed separately.

For the in-plane motions when $n = 2$, Eqs. (27), (28), (32) and (33) can be rewritten in vector–matrix form as

$$\mathbf{M}_I \ddot{\mathbf{X}}_I + \mathbf{C}_I \dot{\mathbf{X}}_I + \mathbf{K}_I \mathbf{X}_I = \mathbf{0}, \quad (35)$$

where \mathbf{M}_I , \mathbf{C}_I and \mathbf{K}_I are the in-plane mass, damping and stiffness matrices, respectively, and

$$\mathbf{X}_I = \{X \ Y \ \gamma \ \phi_1 \ \phi_2\}^T. \quad (36)$$

Note that \mathbf{M}_I , \mathbf{C}_I and \mathbf{K}_I are periodic in time due to the rotation of the spindle motor, and the period of the matrices is $T_I = 2\pi/\omega$.

Similarly, for the out-of-plane motions, Eqs. (29)–(31) can be expressed as

$$\mathbf{M}_O \ddot{\mathbf{X}}_O + \mathbf{C}_O \dot{\mathbf{X}}_O + \mathbf{K}_O \mathbf{X}_O = \mathbf{0}, \quad (37)$$

where \mathbf{M}_O , \mathbf{C}_O and \mathbf{K}_O are the out-of-plane mass, damping and stiffness matrices, respectively, and

$$\mathbf{X}_O = \{Z \ \alpha \ \beta\}^T. \quad (38)$$

It is found that \mathbf{M}_O and \mathbf{C}_O are also periodic in time and they can give rise to parametric instabilities. The period of the out-of-plane mass and damping matrices is $T_O = T_I/2$.

To investigate the stability of the non-autonomous system with the time-dependent periodic coefficients, the Floquet theory [13,14] is used. For convenience of discussion, the following dimensionless parameters are introduced:

$$\bar{\omega} = \frac{\omega}{\omega_0}, \quad \zeta = \frac{2c}{\omega_0(M + M_P)}, \quad \bar{D} = \frac{D}{mR^2\omega_0}, \quad \bar{\varepsilon} = \frac{\varepsilon}{R}, \quad \bar{m} = \frac{m}{M}, \quad (39)$$

where ω_0 is the translational natural frequency of the system as mentioned before. It is almost impossible to consider the stability of the system for the variations of all parameters simultaneously; thus, in this study the stability is analyzed for the variations of pairs of parameters, i.e., $\bar{\omega}$ versus ζ , $\bar{\omega}$ versus \bar{D} , $\bar{\omega}$ versus $\bar{\varepsilon}$, and $\bar{\omega}$ versus \bar{m} , while other parameter values are fixed as shown in Table 1.

The stability of the in-plane motions is first analyzed, and then that of the out-of-plane motions is investigated. First, the Floquet theory is applied to Eq. (35) to evaluate the influence of the energy dissipation factors, c and D , on the stability of the system in the neighbourhood of the balanced equilibrium position for the variations of the rotating speed ω . Shown in Fig. 4 are the stability plots for the dimensionless rotational speed $\bar{\omega}$ versus the damping factor ζ . To obtain the plots, ω and c are varied while other parameter values are fixed. In Fig. 4(a), the maximum values of $|\lambda|$, where λ is the characteristic multiplier [13], are plotted for the various sets of ω and c . In general, a system is stable when $|\lambda|_{\max} < 1$, and the less $|\lambda|_{\max}$, the more stable. Therefore, the three-dimensional plot in Fig. 4(a) shows how stable or unstable the system is. However, the three-dimensional plot cannot clearly visualize the stability boundaries in $\bar{\omega}$ – ζ domain. The two-dimensional plot is thus provided in Fig. 4(b), and only two-dimensional plots will be presented for the stability analysis of other parameter sets. The dotted area is a balanced stable region, and the unmarked area denotes an unbalanced region. It is seen that the system cannot be balanced without damping, and the balanced stable range of $\bar{\omega}$ is increased as ζ increases. It is also observed that the system cannot be balanced when $\bar{\omega}$ is lower than 1. In other words, the ABB does not work when the rotating speed of the spindle motor is lower than the translational natural frequency of the system. This observation is consistent with the results in the literature [6,8]. On the other hand, it is also interesting that an unbalanced region exists around $\bar{\omega} \approx 2$ when ζ is lower than about 0.03. (Note that the values of ζ for metal and rubber suspension washers are 0.025 and

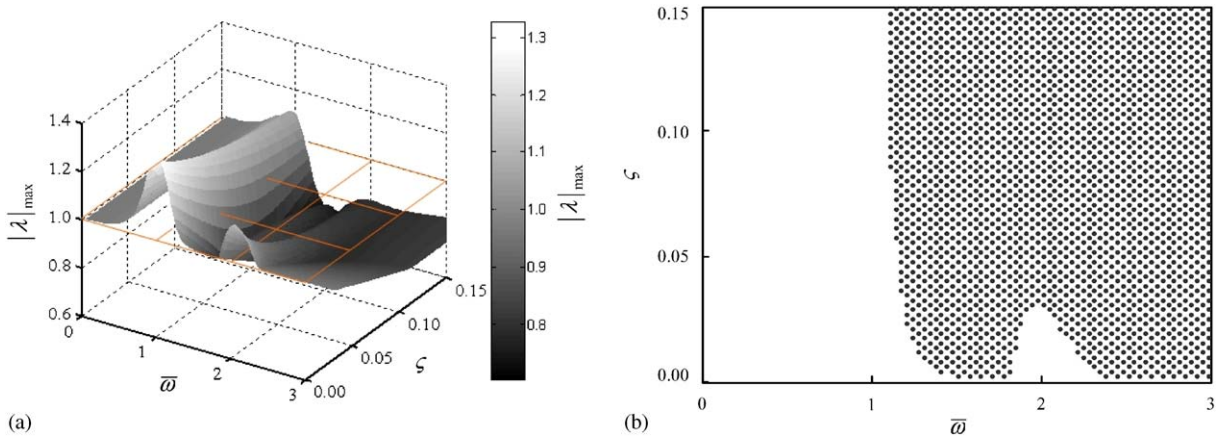


Fig. 4. Stability for the dimensionless rotational speed $\bar{\omega}$ versus the damping factor ζ : (a) three-dimensional plot, (b) two-dimensional plot.

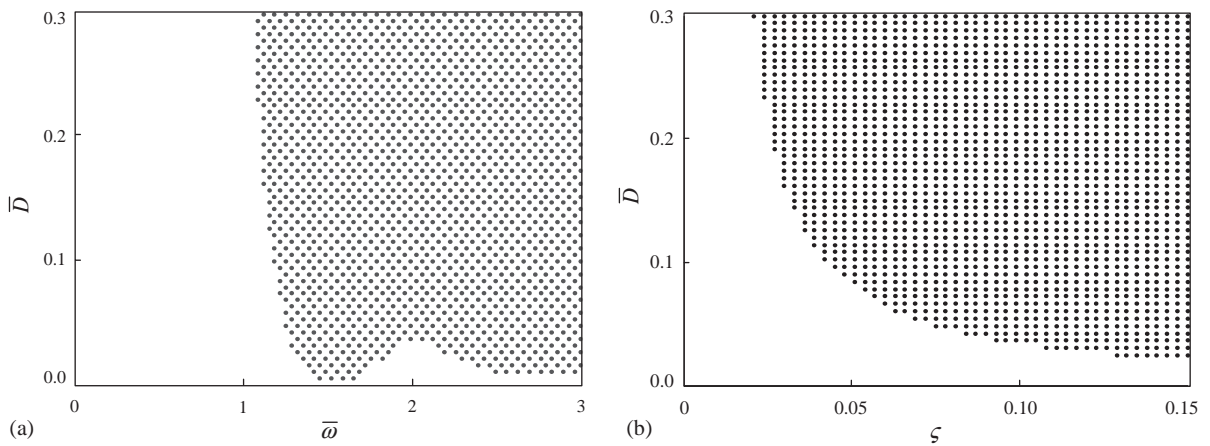


Fig. 5. Stability plots for the dimensionless drag coefficient \bar{D} : (a) $\bar{\omega}$ versus \bar{D} when $\zeta = 0.1$, (b) ζ versus \bar{D} when $\bar{\omega} = 2$.

0.1, respectively [8].) This unbalanced region at $\bar{\omega} \approx 2$ is related to the rotational motion of the feeding deck, and details on the region are discussed in Ref. [10].

Shown in Fig. 5(a) is the stability plot for $\bar{\omega}$ versus the dimensionless drag coefficient \bar{D} . In the simulation, ω and D are varied while other parameter values are fixed as given in Table 1 (the rubber suspension washer is used). It is seen that the shapes of Figs. 4(b) and 5(a) are very similar to each other; thus, the comments made from Fig. 4(b) can also be applied to Fig. 5(a). Both the fluid damping D and the damping of the suspension washers c are essential as energy dissipation factors to obtain balancing. The stability plot for the dampings \bar{D} and ζ (i.e., D and c) when $\bar{\omega} = 2$ is given in Fig. 5(b).

Next, the eccentricity of the rotor system is considered. Fig. 6 is the stability plot obtained by the Floquet theory for $\bar{\omega}$ versus \bar{e} . In the plot, the upper limit of eccentricity which can be balanced

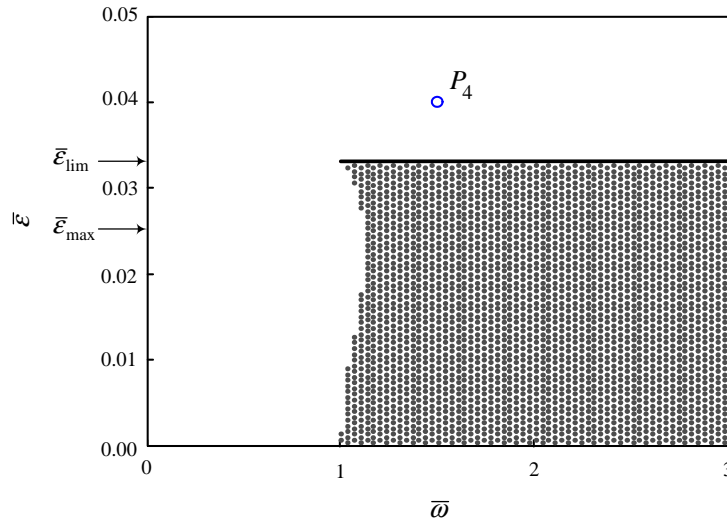


Fig. 6. Stability for the dimensionless rotational speed $\bar{\omega}$ versus the dimensionless eccentricity $\bar{\epsilon}$ when $\zeta = 0.1$.

is denoted by $\bar{\epsilon}_{lim}$. Note that the horizontal solid line corresponding to $\bar{\epsilon}_{lim}$ can also be obtained from Eq. (34) by using the condition that ϕ_1^* and ϕ_2^* exist. It is observed that, in order to obtain balancing, $\bar{\omega}$ should not be lower than 1 and $\bar{\epsilon}$ should be lower than $\bar{\epsilon}_{lim}$. In the design process of commercial CD-ROM or DVD drives, the maximum amount of imbalance, defined by M times ϵ_{max} , is usually assumed as 10 g mm. For the given M the maximum eccentricity ϵ_{max} is about 0.38 mm (i.e., $\bar{\epsilon}_{max} = 0.025$), and the amount should be balanced to satisfy the design specification of the ABB. As shown in Fig. 6, $\bar{\epsilon}_{max}$ can be balanced when $\bar{\omega} > 1.1$ by the balancing balls.

Fig. 7 shows the stability plots for $\bar{\omega}$ versus the mass of a balancing ball \bar{m} . In Figs. 7(a) and (b), the values of ζ are 0.1 (for rubber washers) and 0.025 (for metal washers), respectively, and other parameter values are given in Table 1. The horizontal solid lines, which represent the minimum mass of a balancing ball to achieve balancing for the given values of ϵ , M and R , can also be obtained from Eq. (34). It is seen in Fig. 7(a) that, to be balanced, \bar{m} should be larger than \bar{m}_{lim} , and for a selected \bar{m} the rotating speed ω should be greater than a specific speed related to ω_0 . Similar plots can be found in the studies of the Jeffcott rotor [6] and the two-dimensional optical disk drive [8]. However, the stability plot in Fig. 7(b) for the metal washer has a different shape compared to Fig. 7(a). In Fig. 7(b), new unbalanced regions are found near $\bar{\omega} \approx 2$ inside the balanced region. Special attention is thus needed to guarantee balancing in lower damping cases, for example metal washers. In fact, the speed ($\bar{\omega} \approx 2$) is related to the rotational natural frequencies of the system. Therefore, the result corresponding to Fig. 7(b) could not be obtained by the Jeffcott [6] and two-dimensional [8] models in which the rotational motions were not accounted for.

The Floquet theory is now applied to the out-of-plane equation (37). The stability analyses for the out-of-plane motions are performed to obtain similar plots corresponding to Figs. 4–7 for the in-plane motions. From the analyses for the variations of pairs of parameters, i.e., $\bar{\omega}$ versus ζ , $\bar{\omega}$ versus \bar{D} , $\bar{\omega}$ versus $\bar{\epsilon}$, and $\bar{\omega}$ versus \bar{m} , it is found that the out-of-plane motions are always stable in

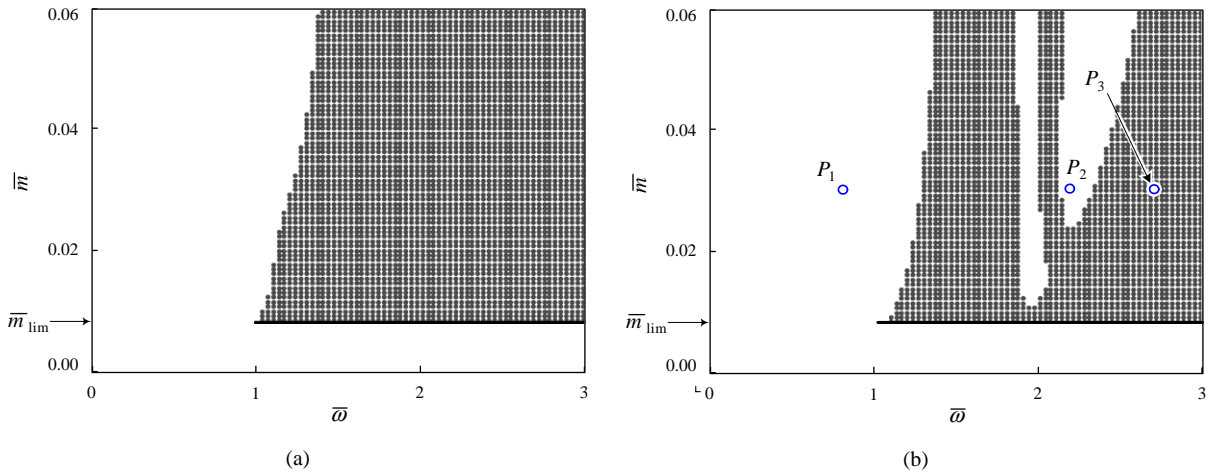


Fig. 7. Stability for the dimensionless rotational speed $\bar{\omega}$ versus the dimensionless mass of a balancing ball \bar{m} when (a) $\zeta = 0.1$, (b) $\zeta = 0.025$.

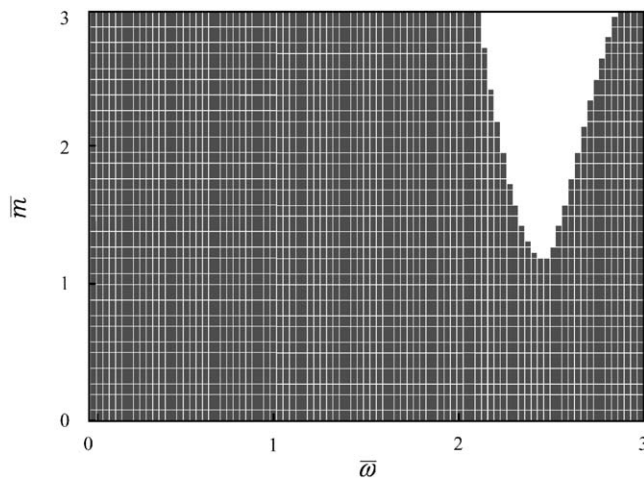


Fig. 8. Stability of the out-of-plane motions for the dimensionless rotational speed $\bar{\omega}$ versus the dimensionless mass of a balancing ball \bar{m} when $\zeta = 0.025$.

the practical regions of all parameter values considered in Figs. 4–7. For example, Fig. 8 shows the stability plot for the out-of-plane motions corresponding to Fig. 7(b) for the in-plane motions. It is seen in Fig. 8 that an unbalanced region occurs around $\bar{\omega} \approx 2.5$ due to parametric resonance. However, the mass of a ball corresponding to the parametric resonance zone is too heavy to be practical. On the other hand, in the practical region of mass (i.e., $\bar{m} < 0.1$), the out-of-plane motions are stable at all $\bar{\omega}$ considered in Fig. 8. Therefore, the stability of the system is determined dominantly by the stability plot of the in-plane motions shown in Fig. 7(b). Similar situations are observed from the stability plots for other parameters. Finally, it can thus be concluded that the

design guidelines distilled from the linearized, in-plane equations of motion can be effectively applied to the ABB installed in optical disk drives in three-dimensional motions.

5. Time responses

The time responses for the motions of the balancing balls and the feeding deck are obtained in order to verify the results of the stability analysis, and to show the performance of ABB. From the nonlinear equations of motion given by Eqs. (18)–(24), the time responses are computed by the Runge–Kutta method. The initial conditions are given as $X(0) = Y(0) = Z(0) = 0.3$ mm, $\alpha(0) = \beta(0) = \gamma(0) = 0^\circ$ and $\phi_1(0) = -\phi_2(0) = 60^\circ$. First, three points in Fig. 7(b), labelled P_1 ($\bar{m} = 0.03$, $\bar{\omega} = 0.8$), P_2 ($\bar{m} = 0.03$, $\bar{\omega} = 2.18$) and P_3 ($\bar{m} = 0.03$, $\bar{\omega} = 2.7$), are considered to verify the stability plot.

Fig. 9 shows the time responses for point P_1 which is located on the unbalanced region. In Fig. 9(a), \bar{r} is the non-dimensionalized displacement of the centre of the rotating system defined by $\bar{r} = \sqrt{X^2 + Y^2 + Z^2}/R$. When the system is balanced, \bar{r} should be zero. However, \bar{r} in Fig. 9(a) approaches a non-zero value. It is seen in Fig. 9(b) that the angular positions of the two balancing balls, ϕ_1 and ϕ_2 , converge to an identical value which means that the balls are overlapped. It is due to the fact that the impact and geometric interference between balancing balls are neglected in the study. Considering these effects, the model could be more precise. However, it may be too complex to perform efficiently the stability analysis. It is also seen that the balls settle down near 0° . It means that the balls are located in the direction of mass imbalance. Thus, as predicted in the stability plot, the system cannot be balanced when the rotating speed is lower than the translational natural frequency.

Shown in Fig. 10 are the responses for point P_2 . The displacement and ball positions do not converge but fluctuate continuously with time since the point P_2 is located in the unbalancing

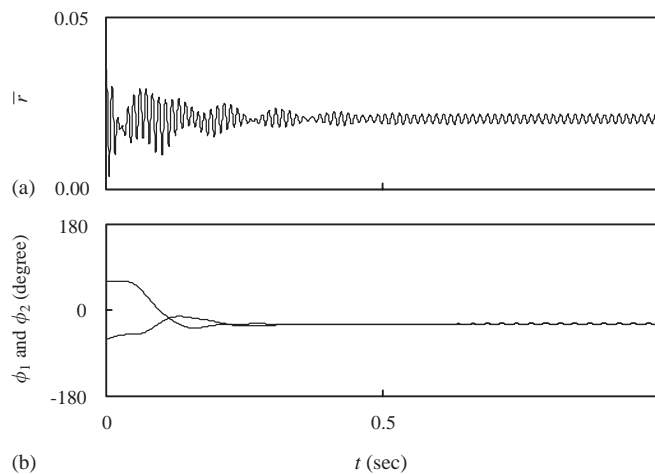


Fig. 9. Time responses for point P_1 : (a) the non-dimensionalized displacement of the centre of the rotating system, (b) the angular positions of the two balancing balls.

zone due to the rotational motion as investigated in the stability analysis. It is seen that the vibrations are very severe; thus, this situation should be avoided.

For the case of point P_3 the non-dimensionalized displacement \bar{r} converges to zero as time increases, as shown in Fig. 11(a). The ball positions in Fig. 11(b) converge to the constant values of about $\pm 106^\circ$. This means that the balancing balls are located in the opposite direction of mass imbalance, and the system is thus balanced as predicted in the stability plot. Recall that the stability plot in Fig. 7(b) is generated from the linearized, in-plane equations of motion. However, the stability plot is verified here by the time responses obtained from the coupled, nonlinear equations considering the three-dimensional motions of the feeding deck. It can be concluded

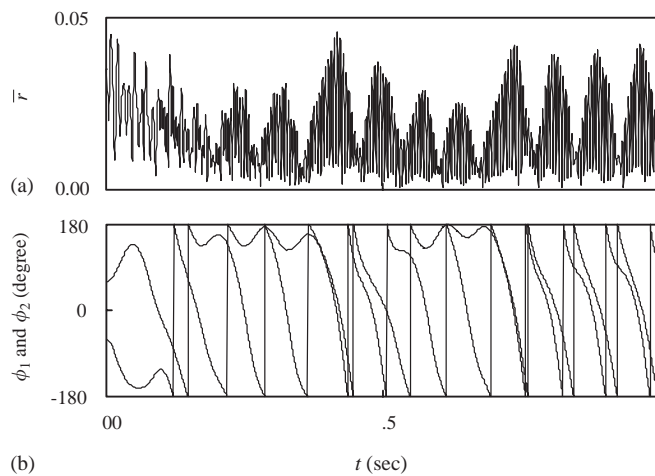


Fig. 10. Time responses for point P_2 : (a) the non-dimensionalized displacement of the centre of the rotating system, (b) the angular positions of the two balancing balls.

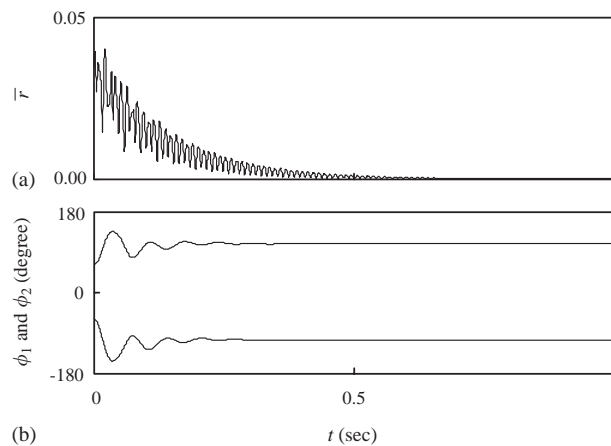


Fig. 11. Time responses for point P_3 : (a) the non-dimensionalized displacement of the centre of the rotating system, (b) the angular positions of the two balancing balls.

that, even though the stability analysis is performed based on the simple linear equations, the results can be effectively used to select the design parameter values of the ABB which can make the three-dimensional system balanced.

To illustrate the performance of the ABB the time responses of point P_3 are presented again. Shown in Fig. 12 are the translational and rotational responses obtained from the nonlinear equations when the ABB is not installed, while shown in Fig. 13 are the responses when the ABB is installed. If there is no ABB, the eccentricity due to mass imbalance makes the in-plane motions of system vibrating as shown in Figs. 12(a), (b) and (f). However, if the ABB is working, the in-plane translational vibrations disappear as shown in Figs. 13(a) and (b). The in-plane rotational angle γ shown in Fig. 13(f) also converges to zero when the ABB enables the system to be balanced. On the other hand, shown in Figs. 12(c)–(e) and 13(c)–(e) are the out-of-plane time

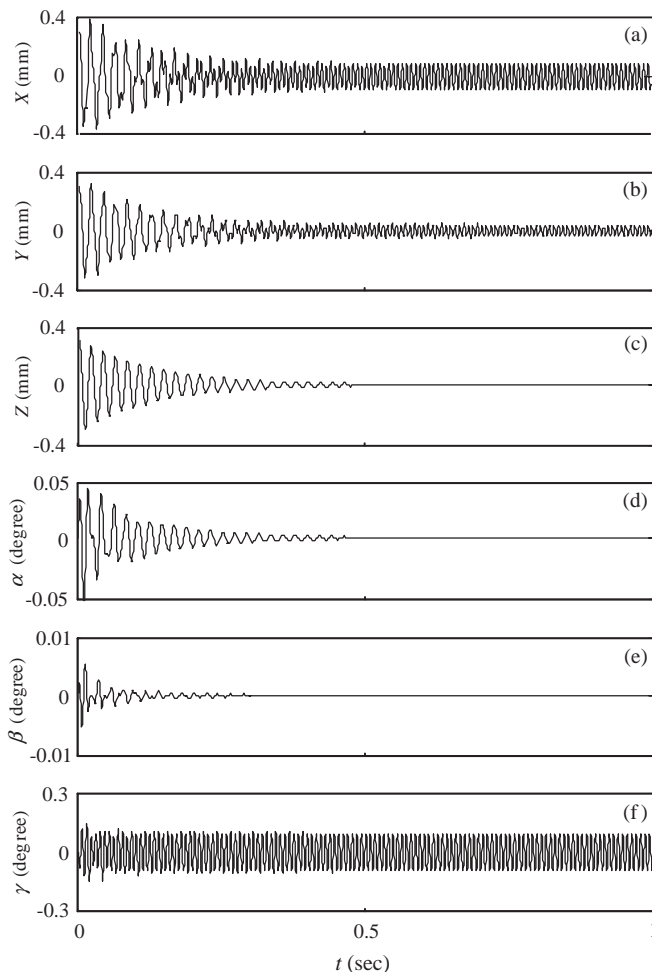


Fig. 12. Time responses for point P_3 when the ABB is not installed: (a) the in-plane translational displacement X , (b) the in-plane translational displacement Y , (c) the out-of-plane translational displacement Z , (d) the out-of-plane rotational angle α , (e) the out-of-plane rotational angle β , (f) the in-plane rotational angle γ .

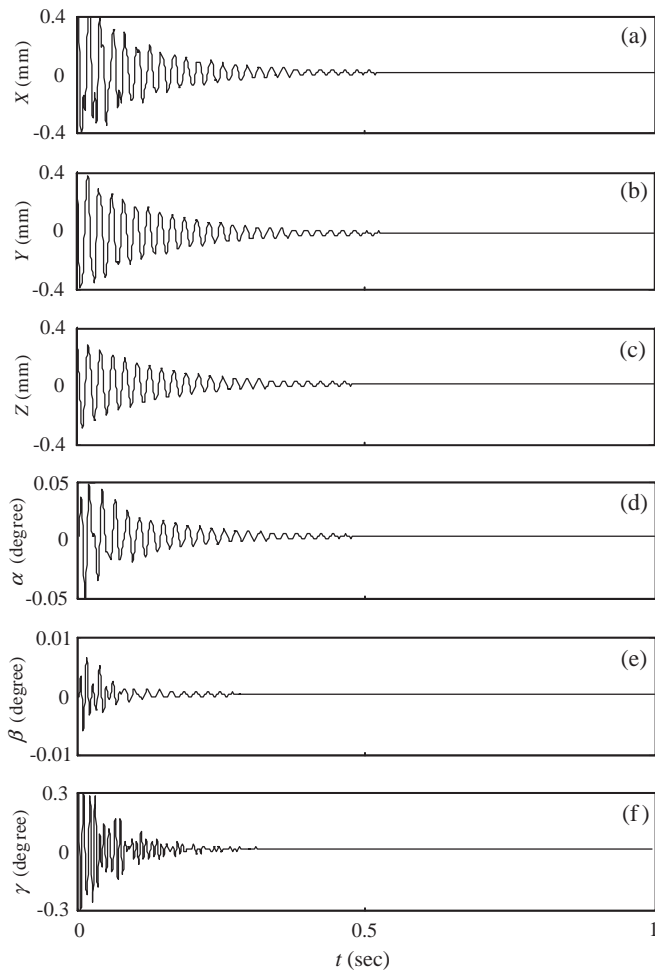


Fig. 13. Time responses for point P_3 when the ABB is installed: (a) the in-plane translational displacement X , (b) the in-plane translational displacement Y , (c) the out-of-plane translational displacement Z , (d) the out-of-plane rotational angle α , (e) the out-of-plane rotational angle β , (f) the in-plane rotational angle γ .

responses. Note that all the out-of-plane vibrations diminish with time regardless of the existence of the ABB. Therefore, it is believed that a dominant player to damp out the out-of-plane motions is not the ABB but energy dissipation by the suspension washers. However, it can also be noticed in this case that at least the ABB does not make the out-of-plane motions grow, although it does not contribute toward eliminating the vibrations.

At this stage, it is valuable to make one more comment regarding the effects of the ABB on the out-of-plane motions. Recall that all the mass centres are assumed to be on the same plane in the modelling process because the latest optical disk drives are slim. However, if the more general case, in which the mass centres are located on the different planes, is considered, a modified three-dimensional model of the feeding deck and rotor system may need to be developed as mentioned in Section 2. In addition, the ABB may have influences on the out-of-plane vibrations in this case

(see Ref. [11] for the order of magnitude of the tilting angle: 0.0000476° for the typical system with an ABB). To make the general system balanced perfectly, the authors suggest using two ABBs on the different planes. This type of balancing is often called the two-plane balancing. However, the modelling and analysis methods for the case are believed to be almost the same as those in this study. Therefore, the procedure used in this study can also be adopted easily and effectively in the two-plane balancing analysis.

Now, a special situation, in which the mass unbalance is greater than the balancing capacity of the balancing balls, is briefly investigated. Fig. 14 shows the time responses for the point P_4 ($\bar{\varepsilon} = 0.04, \bar{\omega} = 1.5$) in Fig. 6. As predicted in Fig. 6, the system having the parameter values of P_4 cannot be balanced since the unbalance amount is greater than $\bar{\varepsilon}_{\text{lim}}$. However, it is noticed in Fig. 14 that the magnitude of the residual vibration of the system with the ABB is much smaller than that of the system without the ABB. Therefore, the use of the ABB is still beneficial although the system is not perfectly balanced.

Lastly, the time responses when the number of balancing balls $n = 10$ will be presented since, as mentioned before, about ten balls are usually used in the ABB for an optical disk drive. As an example, the case of point P_3 in Fig. 7(b) is considered. Recall that the point P_3 has been predicted as a stable point when $n = 2$, and the corresponding time responses have been shown in Fig. 11. For $n = 10$ the time responses are shown in Figs. 15 and 16: (a) the non-dimensional displacement \bar{r} and (b) the positions of ten balancing balls versus time. It is seen that the initial positions of ten balls in Fig. 15(b) are close to $\pm 60^\circ$ while those in Fig. 16(b) are scattered within the race. For reasonable comparisons the total mass of balancing balls is given to be the same in all cases (Figs. 11, 15 and 16). First of all, in Figs. 15(a) and 16(a), the displacement \bar{r} converges to zero as time increases, and the system is finally balanced as predicted in Fig. 7(b) for $n = 2$. Also, the magnitude of displacement and the converging time in Figs. 15(a) and 16(a) are very similar to those in Fig. 11(a). Therefore, the analysis results based on the two-ball assumption may be effectively used for the design of an ABB having many balancing balls. It is also seen that the steady-state locations of the balancing balls in Fig. 15(b) are similar to those in Fig. 11(b) because the initial positions of the balls are almost the same in both simulations. However, the steady-state locations of the balancing balls in Fig. 16(b) are different from those in Fig. 15(b). It means that the equilibrium positions of the balancing balls when $n = 10$ are not unique, and depend on initial conditions. This situation usually makes the stability analysis more complex. The analysis procedure studied in this article using two balancing balls can thus be an alternative to the problem.

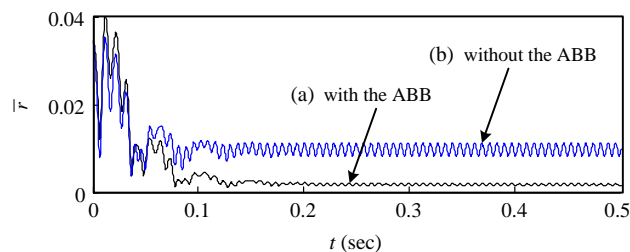


Fig. 14. Time responses for point P_4 : (a) when the ABB is installed, (b) when the ABB is not installed.

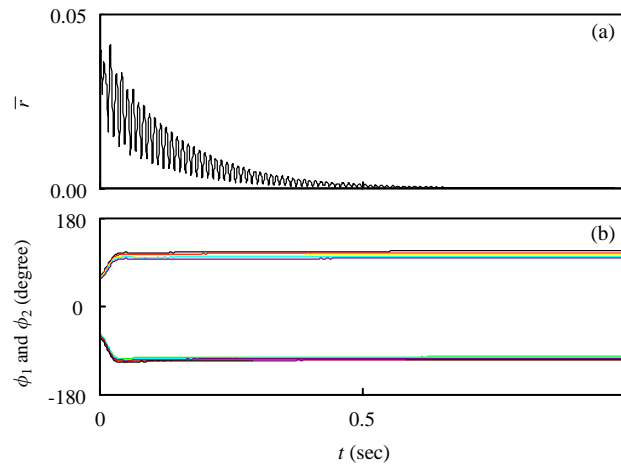


Fig. 15. Time responses for point P_3 when $n = 10$ and the initial positions of the ten balls are close to $\pm 60^\circ$: (a) the non-dimensionalized displacement of the centre of the rotating system, (b) the angular positions of the balancing balls.

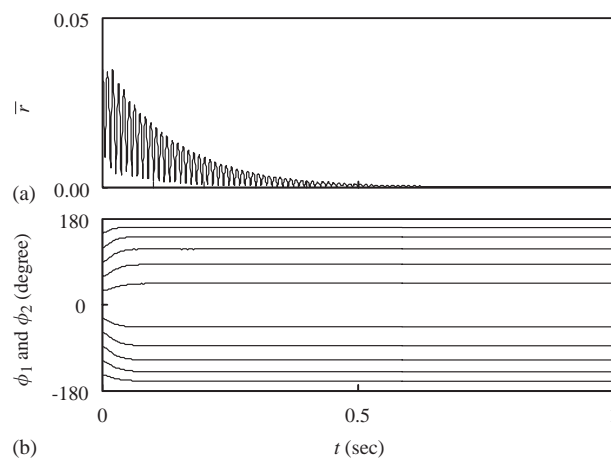


Fig. 16. Time responses for point P_3 when $n = 10$ and the initial positions of the ten balls are scattered: (a) the non-dimensionalized displacement of the centre of the rotating system, (b) the angular positions of the balancing balls.

6. Summary and conclusions

A dynamic model is developed for a commercial optical disk drive with an automatic ball balancer, considering the translational and rotational motions in the three-dimensional space. From the model, the coupled nonlinear equations of motion are derived by using Lagrange's equation. Applying the perturbation method to these equations, linearized equations in the vicinity of the equilibrium position as well as a balanced equilibrium position are obtained. The perturbed linear equations are categorized into two independent groups for the small motions of the in-plane and the out-of-plane. Based on the equations of each group, the stability analyses are

performed by using the Floquet theory because the equations have time-dependent periodic coefficients. The stability plots are presented for some parameters of the system, for example, rotating speed, ball mass, eccentricity and damping, to investigate their effects on the balancing performance of the ABB. The time responses for the three-dimensional motions of the feeding deck are also computed from the nonlinear equations of motion to verify the results of the stability analysis.

It is observed from the stability plots and time responses that the dynamics of the ABB is deeply related to not the out-of-plane but the in-plane motions. It can thus be concluded that the two-dimensional, in-plane model instead of the three-dimensional full model can be effectively used for predicting balancing regions and for selecting ABB parameters in a design process. In fact, the analysis based on only the in-plane motions is much simpler and faster than that of the three-dimensional motions. However, the in-plane rotational motion should not be neglected in the in-plane model to account for unbalanced regions related to the rotational natural frequency of the system. It has been well known from the literature that the rotating speed should be greater than the translational natural frequency to be balanced by the ABB. However, it is observed in this study that the criterion for the translational natural frequency could not guarantee the balancing of an optical disk drive. An important point which has to be added to the guidelines of the literature is that not only the translational but also the rotational natural frequencies should be considered when operating speeds are selected.

Acknowledgements

The authors are grateful for the financial support provided by a grant (Grant Number: R01-2000-000-00292-0 (2002)) from the Korea Science and Engineering Foundation (KOSEF).

References

- [1] S. Bae, J.M. Lee, Y.J. Kang, J.S. Kang, J.R. Yun, Dynamic analysis of an automatic washing machine with a hydraulic balancer, *Journal of Sound and Vibration* 257 (2002) 3–18.
- [2] C. Rajalingham, S. Rakheja, Whirl suppression in hand-held power tool rotors using guided rolling balancers, *Journal of Sound and Vibration* 217 (1998) 453–466.
- [3] J.D. Alexander, An automatic dynamic balancer, in: *Proceedings for the Second Southeastern Conference*, Vol. 2, 1964, pp. 415–426.
- [4] J.W. Cade, Self-compensating balancing in rotating mechanisms, *Design News* (1965) 234–239.
- [5] J. Lee, W.K. Van Moorhem, Analytical and experimental analysis of a self-compensating dynamic balancer in a rotating mechanism, *Journal of Dynamic Systems, Measurement, and Control* 118 (1996) 468–475.
- [6] J. Chung, D.S. Ro, Dynamic analysis of an automatic dynamic balancer for rotating mechanisms, *Journal of Sound and Vibration* 228 (1999) 1035–1056.
- [7] H. Hwang, J. Chung, Dynamic analysis of an automatic ball balancer with double races, *JSME International Journal* 42 (1999) 265–272.
- [8] J.-R. Kang, C.-P. Chao, C.-L. Huang, C.-K. Sung, The dynamics of a ball-type balancer system equipped with a pair of free-moving balancing masses, *Journal of Vibration and Acoustics* 123 (2001) 456–465.
- [9] W.-Y. Huang, C.-P. Chao, J.-R. Kang, C.-K. Sung, The application of ball-type balancers for radial vibration reduction of high-speed optic disk drives, *Journal of Sound and Vibration* 250 (2002) 415–430.

- [10] W. Kim, J. Chung, Performance of automatic ball balancers on optical disk drives, *Journal of Mechanical Engineering Science* 216 (2002) 1071–1080.
- [11] P.C.P. Chao, Y.-D. Huang, C.-K. Sung, Non-planar dynamic modeling for the optical disk drive spindles equipped with an automatic balancer, *Mechanism and Machine Theory* 38 (2003) 1289–1305.
- [12] C. Rajalingham, R.B. Bhat, S. Rakheja, Automatic balancing of flexible vertical rotors using a guided ball, *International Journal of Mechanical Sciences* 40 (1998) 825–834.
- [13] L. Meirovitch, *Methods of Analytical Dynamics*, McGraw-Hill, New York, 1970 (Chapter 7).
- [14] C. von Kerczek, S.H. Davis, Calculation of transition matrices, *AIAA Journal* 13 (1975) 1400–1403.